The nature of the light absorption and emission transitions of 4-hydroxybenzophenone in different solvents. A combined computational and experimental study

The nature of the light absorption and emission transitions of 4-hydroxybenzophenone in different solvents. A combined computational and experimental study.

Francesco Barsotti,[a] Giovanni Ghigo,[b,]* Silvia Berto,[a] Davide Vione [a,]*

Dipartimento di Chimica, Università di Torino, Via Giuria 5[a] and/or 7[b], 10125 Torino, Italy.

* Address correspondence to either author: *giovanni.ghigo@unito.it* (G. Ghigo, Phone +39-011-6707872), *davide.vione@unito.it* (D. Vione, Phone +39-011-6705296)

Abstract

The photophysics and photochemistry of 4-hydroxybenzophenone (4HOBP) are interesting because they can give some insight into the behavior of humic material. Here we show that 4HOBP has a number of fluorescence peaks: *(i)* an intense one at excitation/emission wavelengths Ex/Em ~200-230/280-370 nm, likely due to an excitation transition from S_0 to S_5 or S_6, followed by $S_2 \rightarrow S_0$ in emission (S_n denote the singlet states of 4HOBP); *(ii)* a minor peak at Ex/Em ~270-300/320-360 nm ($S_0 \rightarrow S_2$ in absorption and $S_2 \rightarrow S_0$ in emission), and *(iii)* very interesting signals in the typical emission region of humic substances, most notably at Ex/Em ~200-220/400-500 nm and Ex/Em ~260-280/400-470 nm (in both cases the emission corresponded to a $S_1 \rightarrow S_0$ transition). The peak *(i)* (Ex/Em ~200-230/280-370 nm) is quite intense at low 4HOBP concentration values, but it undergoes an effective inner-filter phenomenon. Remarkably, 4HOBP shows fluorescence peaks that derive from $S_2 \rightarrow S_0$ transitions and that do not follow Kasha's rule. Fluorescence is observed in aprotic or poorly protic solvents, and to a lesser extent in aqueous solution. The excited states of 4HOBP, and most notably 4HOBP-S_1, are much stronger acids than 4HOBP-S_0. Therefore, excited 4HOBP is quickly deprotonated to 4OBP$^-$-S_0 in ~neutral solution, with a considerable loss of the fluorescence properties. Higher fluorescence intensity can be observed under acidic conditions, where excited-state deprotonation is less effective, and in basic solution where the dissociated 4OBP$^-$-S_0 form prevails as the ground state. The excited states of 4OBP$^-$ are formed directly upon radiation absorption, and being weak bases they do not undergo important acid-base equilibria. Therefore, they can undergo radiational deactivation to produce a significant fluorescence emission.

Keywords: Excitation-emission fluorescence matrix; phototransformation; density functional theory; Kasha's rule.

1. Introduction

The 4-hydroxybenzophenone (4HOBP) is an interesting compound for photochemistry studies because its ground singlet state is a weak acid with pK_a ~ 8,[1] while the excited singlet and triplet states are strong acids. This issue significantly affects the photoluminescent and photochemical behavior of 4HOBP in protic solvents and particularly in aqueous solution, where undissociated 4HOBP absorbs radiation and its excited states undergo quick deprotonation, to give at some stage the anionic species $4OBP^-$ in its ground state. The latter is readily protonated to produce the starting compound 4HOBP.[2-4] In the overall process the photon energy is lost non-radiationally, which explains a number of observations: *(i)* the fluorescence intensity of 4HOBP is much higher in aprotic solvents than in water;[3] *(ii)* the first excited triplet state of 4HOBP is easily detected by laser flash photolysis in aprotic solvents, but it is not detected in aqueous solution;[2-8] *(iii)* 4HOBP is a rather efficient photosensitizer that induces the photodegradation of other compounds in aprotic or weakly protic solvents, but its photosensitizing ability is lost in aqueous solution.[3,9] Interestingly, most of the cited aqueous-solution studies have been carried out at ~neutral pH.

Another interesting feature of 4HOBP is that its fluorescence spectrum shows a peak at excitation wavelengths around 300 nm and emission wavelengths above 400 nm,[3] which remarkably overlaps with the so-called "peak C" of humic substances.[10,11] Indeed, a very fast, cheap and efficient way to detect the occurrence of humic compounds in natural water samples is to use the fluorescence spectroscopy and, most notably, the excitation-emission matrix (EEM) technique. In the presence of humic material, two peaks at excitation/emission wavelengths Ex/Em = 230-260/400-500 and 300-350/400-500 nm are usually observed, respectively named "peak A" and "peak C".[10,11] Surprisingly, the fluorescence spectrum of 4HOBP has been reported only very recently,[3] and a detailed mechanistic understanding of its features is still missing. The fluorescence properties of humic substances are widely used to characterize surface water samples and to assess the origin and environmental processing of the organic matter they contain,[12-15] but the actual reasons behind the fluorescence emission of the humic material are still very elusive. Fluorescence emission wavelengths around 500 nm could be accounted for by phenol oligomers,[16] but it is clear that any compound with fluorescence emission in the region(s) of "peak A" and/or "peak C" of humic substances deserves particular attention. A detailed understanding of the relevant photophysical pathways can help elucidating the nature of the transitions behind humic fluorescence. Another reason that could make 4HOBP an interesting model for the photochemistry of humic compounds is that the latter are probably aggregates of smaller molecules,[17,18] where the most hydrophilic ones are located at the surface in contact with water, and the hydrophobic ones form a waterless inner core. The hydrophobic cores of humic substances are locations where an unusually elevated concentration of $^1O_2$ can be detected under illumination (much higher compared to the solution bulk [19,20]), which could play an important role in the photochemical degradation of hydrophobic

pollutants. There is evidence that part of the reason for the elevated $^1O_2$ concentration in hydrophobic cores is that the lifetime of $^1O_2$ is higher in waterless environments.[21,22] However, a compound such as 4HOBP is interestingly able to produce $^1O_2$ when irradiated in aprotic or weakly protic solvents, but no $^1O_2$ photoproduction takes place in water.[3] Considering that benzophenone derivatives are quite common in natural humic material,[23,24] compounds like 4HOBP might contribute to elevated $^1O_2$ levels in hydrophobic environments while their photoreactivity would be quenched at the interface with water.

The electronic structure of the first excited states of 4HOBP, in particular S_1 and T_1, has been the object of early studies.[7,8] Labels like $n\pi^*$ and $\pi\pi^*$ have been used to name these states based, in part, on their capability to abstract hydrogen atoms from suitable substrates (phenols and benzyls).[25] Moreover, the nature and energy position of these states is sensitive to the polarity and hydrogen-bond forming capability of the solvent.[4,6] However, although very attractive, the description of the excited states as a single configuration generated by only one electronic excitation from an occupied molecular orbital to a virtual molecular orbital is too coarse. The excited states often show a multiconfigurational nature, i.e. they are described by several electronic configurations each corresponding to different excitations from occupied to virtual orbitals (where the HOMO-LUMO transition is only one of them). In this work we intend to analyze the electronic structure of the excited states with a more accurate approach, based on the analysis of the change of the electronic density going from the ground to the excited states. The electronic densities of the latter are obtained through the combination of the coefficients of the configurations, as found in the TD-DFT outputs and the molecular orbitals. This allows a graphic representation of the difference in electronic densities between the ground and the excited state. Moreover, this work aims at elucidating the nature of the transitions leading to the observed absorption and, most notably, fluorescence spectrum of 4HOBP.

2. Materials and methods

Solutions of 4-hydroxybenzophenone (Acros Organics, >99%) were prepared in water (Milli-Q quality, resistivity 18 MΩ cm, DOC < 0.01 mg L^{-1}), acetonitrile (Aldrich, 99.9% HPLC gradient grade) and 2-propanol (Aldrich, >98%). In some experiments, the pH value of the aqueous solutions was adjusted with $HClO_4$ (Aldrich, 65% w/w) or NaOH (Aldrich, >98% reagent grade) and it was measured with a Metrohm 602 combined glass electrode, connected to a Metrohm 713 pH meter. When required, oxygen-free and pure-oxygen atmospheres were obtained by purging the solutions with a gentle flow of, respectively, Ar (Sapio, Monza, Italy, grade 5.5, 99.9995%) and O_2 (Sapio, grade 2.5, 99.5%).

The absorption spectra of 4-hydroxybenzophenone (4HOBP) were measured with a Varian Cary 100 Scan UV-Vis double-beam spectrophotometer, using quartz cuvettes (Hellma, 1.000 cm optical path length). The excitation-emission matrix (EEM) fluorescence spectra were taken with a VARIAN Cary Eclipse Fluorescence Spectrofluorimeter, with an excitation range from 200 to 400 nm at 10 nm steps, and an emission range from 200 to 600 nm with a scan rate of 1200 nm min^{-1}. Other emission spectra were measured upon excitation at a single wavelength, and the excitation spectra were taken by fixing the emission wavelength while varying the excitation one. All the spectra were measured in a fluorescence quartz cuvette (Hellma) with 1.000 cm optical path length. The Raman signal of water was taken as a reference for lamp intensity and signal stability within different measurements.

The computational study was performed within the Density Functional Theory (DFT)[26-28] with the Pople basis set 6-31+G(d).[29,30] Solvent effects (ACN, 2-propanol and water) to the electronic energies were introduced in all calculations (ground and excited state optimizations and single point calculations) by the Polarized Continuum Method (PCM)[31,32] within the universal Solvation Model Density.[33,34] The absorption spectra were obtained with the following procedure: we first optimized the geometries of the ground states, then we calculated the excitation energies with the Time-Dependent DFT (TD-DFT).[35,36] This method provides a reasonable accuracy at reasonable computational costs (time and computing resources).[37-40] On the basis of the literature and after a few tests on the absorption in ACN (**Figure ESI1** in the Electronic Supplementary Information, hereafter ESI) we decided to use the functional PBE0.[41-43] The excitation energies calculated in this way correspond to the maxima in the absorption spectra, as this approach does not include vibrational contributions or dynamic solvent effects. The absorption spectra of 4HOPB in the three solvents were obtained through linear combination of gaussian functions centered on the calculated electronic transition frequencies, with relative height calculated from the oscillator strength as explained in references 44 and 45. The geometry of 4HOBP was re-optimized in its excited states (singlet and triplet), and the difference between the energies of these states and those calculated for the ground state at the excited state geometries was taken as emission (fluorescence) energy. For the proton transfer equilibria, the energies were refined through single-point calculations with the 6-311+G(d,p) basis set[46] and combined with the 6-31+G(d) thermal corrections to the free energy. Calculations were performed using the quantum package Gaussian 09-A.[47] **Figures 6 and 7** and **Figures ESI6, ESI7 and ESI8** were obtained with the graphical program Molden.[48] **Figures 1a, 5 and 8b** and **Figure ESI1** were obtained with the graphical program GNUPlot.

3. Results and Discussion

3.1 Absorption and emission spectra

The absorption spectra of 4HOPB in three different solvents (**Figure 1a**) were obtained from the electronic transitions from the ground state (S_0), calculated at the TD-DFT level. The agreement with experimental data (**Figure 1b**) is remarkably good. The three main signals observed in acetonitrile (ACN) are well reproduced: the peak found at 283 nm (Du *et al.* report 284 nm)[2] is calculated at 288 nm and corresponds to a $S_0 \rightarrow S_2$ transition (oscillator strength f= 0.405, see **Table ESI1.1b**); the bump found at 249 nm (250 nm, Du *et al.*)[2] is calculated at 252 nm ($S_0 \rightarrow S_5$, f= 0.151); the bump found at 221 nm (222 nm, Du *et al.*)[2] is a combination of transitions calculated at 230 ($S_0 \rightarrow S_6$, f= 0.0891) and 220 nm ($S_0 \rightarrow S_7$, f= 0.0684). The strong absorption below 210 nm, well reproduced by the calculations, is a combination of several transitions calculated at 194 and 193 nm (with participation of other less intense transitions, see **Table ESI1.1b**). A weak absorption (f= 0.005) corresponding to the $S_0 \rightarrow S_1$ transition is also calculated at 327 nm but the strong band at 283 nm partially hides it. Clear traces of this transition can be found in the tail of the stronger band in the experimental spectrum, so it is possible that the calculation underestimates its oscillator strength.

The bathochromic effect on the lower energy transition, due to protic solvents (2-propanol and water), is also reproduced.[3] The maxima found at 294 (2-propanol) and 296 nm (water) are calculated with an error of 2 nm, respectively, at 292 and 294 nm (both $S_0 \rightarrow S_2$ transitions). The bumps found at 249 nm (2-propanol) and 260 nm (water) are calculated at 255 and 257 nm (both $S_0 \rightarrow S_5$ transitions), while those found at 230 nm (2-propanol) and 226 nm (water) are combinations of transitions calculated, respectively, at 230 and 210 nm and at 229 and 218 nm. As for ACN, the $S_0 \rightarrow S_1$ transitions (321 nm in 2-propanol and 317 nm in water) are predicted to be very weak (f=0.008 and 0.011). Indeed, the solvent effect does not seem to be very remarkable (~0.1 eV), but this is possibly due to the fact that the studied solvents are all already quite polar. Larger effects have been observed by comparing pure apolar cyclohexane with alcohols-cyclohexane mixtures.[4]

The optimization in ACN of the structures of the excited states allowed the calculation of the electronic transitions from these states to the ground state S_0. These transitions, that should correspond to the emission spectra, are calculated at: *(i)* 521 nm from the first triplet state T_1; *(ii)* 504 nm from the first singlet excited state S_1; and *(iii)* 337 nm from the second singlet excited state S_2. For the triplet state T_1 the absorption spectrum in ACN was also calculated (see **Table ESI1.4b** and **Figure 1c**), finding two intense transitions at 319 and 498 nm. These are in quite good agreement with the absorption maxima at 330 and 520 nm registered in the laser flash photolysis (LFP) experiments reported in our previous paper,[3] and with 518 nm reported by Mittal *et al.* [6]

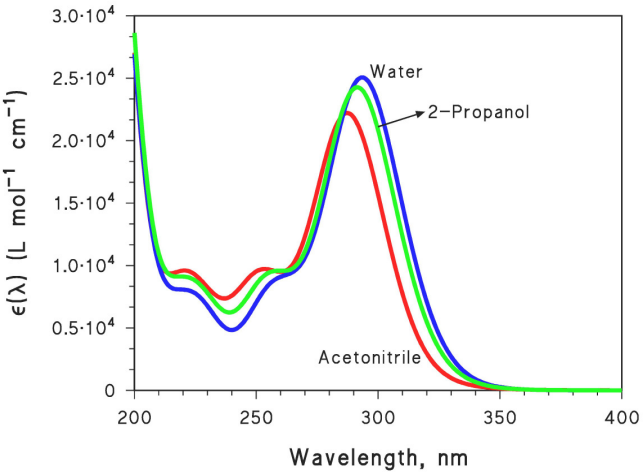

(a)

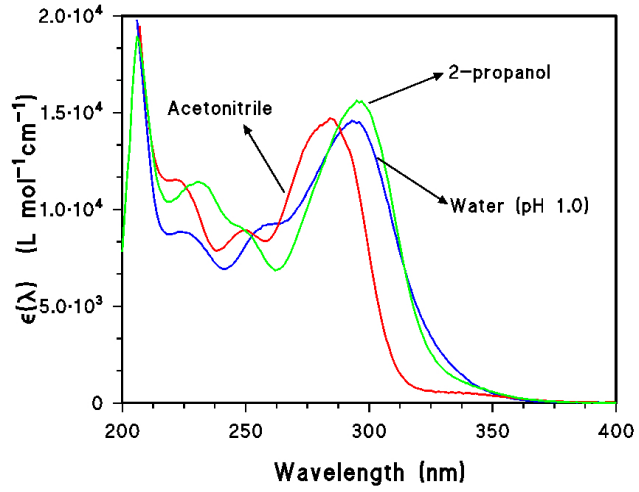

(b)

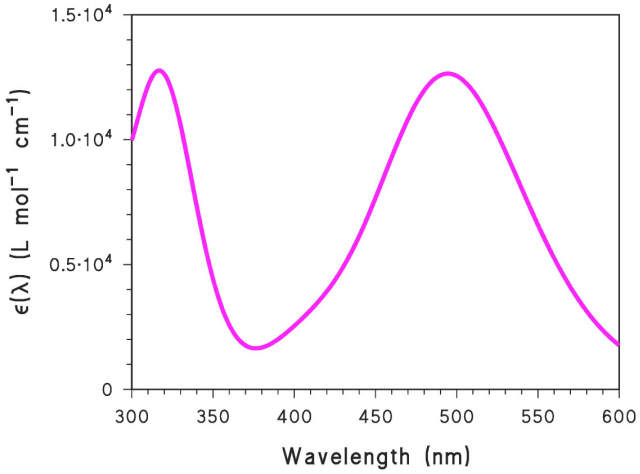

(c)

Figure 1. Calculated **(a)** and experimental **(b)** absorption spectra of 4HOBP in ACN (red line), 2-propanol (green line) and water (blue line), the latter with pH adjusted to 1.0 with $HClO_4$. **(c)** Calculated absorption spectrum of the T_1 excited state of 4HOBP in ACN.

Figure 2 shows a semi-quantitative picture of the potential energy curves of the S_1, S_2 and T_1 excited states and of the ground state S_0 (details can be found in ESI). Vertical dashed lines in **Figure 2** represent the radiative transitions. Arrows pointing upward are absorptions leading to the excited states and starting from the minimum of the energy curve of S_0. Arrows pointing downwards, starting from the minima of the excited states and reaching the S_0 potential curve, represent the emission. R is an arbitrary parameter representing the geometrical distortion from the equilibrium geometry of the ground state. Further details on how **Figure 2** was obtained and on the exact meaning of the R parameter are reported in ESI, page 4.

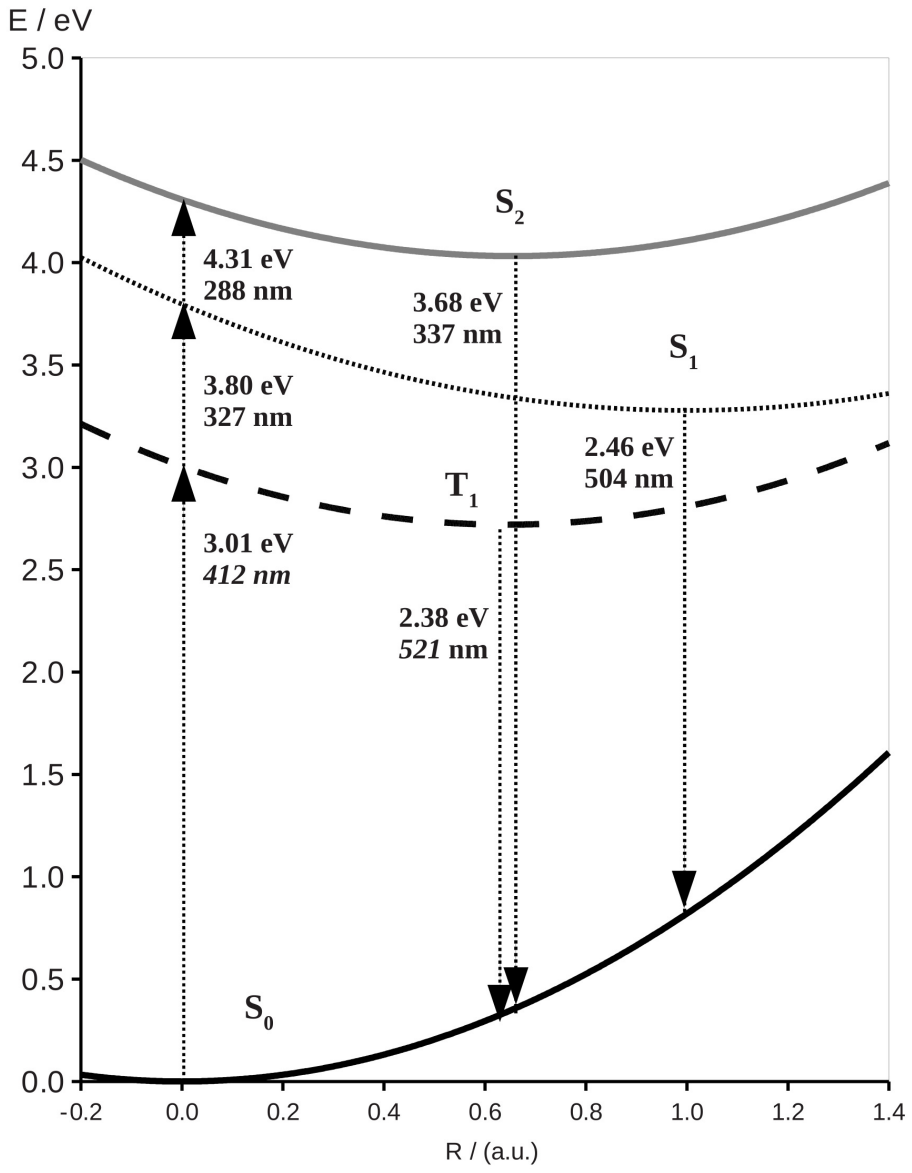

Figure 2. Potential energy curves (in eV) of states S_0, S_1, S_2, and T_1 as a function of the arbitrary parameter R (arbitrary unit, a.u.), representing the geometrical distortion from the equilibrium geometry of the ground state. Values in eV and nm refer to radiative transitions (see text and ESI).

Although approximate, this picture relates with the actual change of the optimized structures of the excited states with respect to the starting geometry, which corresponds to the ground state. **Figure ESI2** reports the most important geometrical parameters of S_0, S_1, S_2 and T_1, along with the standard deviations (in atomic units, a.u.) of the geometries of the excited states with respect to S_0. The standard deviations are 0.068 a.u. for T_1 (R is 0.642); 0.083 a.u. for S_2 (R is 0.655); 0.297 a.u. for S_1 (R is 1). These data confirm that R and the standard deviations are of the same order (although not linearly correlated). A precise correlation among the standard deviations and the parameter R is impossible because the potential energy surfaces are intrinsically multidimensional. However, we can observe that the largest contributions to the structural changes are given by the dihedral angles between the phenyl rings (Θ_A and Θ_B in **Figure ESI2**). In particular, Θ_B changes from -24 in S_0 to -87 in S_1. This large variation makes the simulation of the fluorescence from state S_1 particularly difficult. This problem is also the reason why the inclusion of the Franck-Condon factors in the simulation of the fluorescence of biphenyl was found problematic by Mennucci, Adamo and Jacquemin,[40] and possibly it is an explanation of the large peak found in the "C-like" area of the EEM spectra.[3]

The raw emission spectrum of 4HOBP in ACN showed important changes as a function of 4HOBP concentration. At quite low 4HOBP levels (e.g. 0.01 mM, **Figure 3a**) there is a major peak at Ex/Em = 200-230/280-370 nm and a relatively small peak at Ex/Em = 270-300/320-360 nm. The occurrence of two separate peaks is highlighted in the excitation spectrum reported in **Figure 3b**, which corresponds to the emission wavelength of 350 nm. Highlighted on the latter figure are also signals that do not depend on 4HOBP, such as the Rayleigh scattering and the Raman signal of water. Comparison with TD-DFT computations suggests that the emission found at 280-370 or 320-360 nm could be assigned to the $S_2 \rightarrow S_0$ transition, calculated at 337 nm. To support this hypothesis we must note that, at the variance with state S_1, state S_2 shows a higher oscillator strength (0.472, compared to 0.001) and its geometry is closer to that of the ground state (see **Figure 2** and text above), determining a larger Franck-Condon factor. All these factors should increase the probability of decay from state S_2 through a radiative transition. This suggests that 4HOBP does not follow Kasha's rule,[49] according to which the fluorescence emission takes place from the lowest excited state (S_1). Although quite uncommon, emissions from excited states upper than S_1 and violating the Kasha's rule have already been observed.[50,51] The molecule closer to our system is *o*-hydroxybenzaldehyde, which showed fluorescence from the S_2 state.[52]

According to the calculation results reported in **Figure 2** the state S_2 should be reached upon absorption of radiation at 288 nm, but the main fluorescence peak was centered at the excitation wavelengths of 200-230 nm. This may be consistent with an excitation to vibrationally excited S_2, followed by radiationless vibrational decay and by radiative emission. However, coherently with both experimental and computational data, a different rationalization for the main fluorescence peak

could be put forward: it could be due to an excitation to S_5 or S_6 states (the respective electronic transitions are calculated at 252 and 230 nm, with oscillator strengths of 0.150 and 0.089), followed by radiationless decay through internal conversion to S_2. The small peak in the EEM spectrum at 270-300/320-360 nm corresponds to the peak at 280-290 nm in **Figure 3b**, in agreement with calculations, and is consistent with a $S_0 \rightarrow S_2$ transition in excitation and with $S_2 \rightarrow S_0$ in emission. Because the two peaks are clearly distinct in both the EEM and excitation spectra, the hypothesis that the most intense one is due to a $S_0 \rightarrow S_5/S_6$ transition in absorption looks more likely.

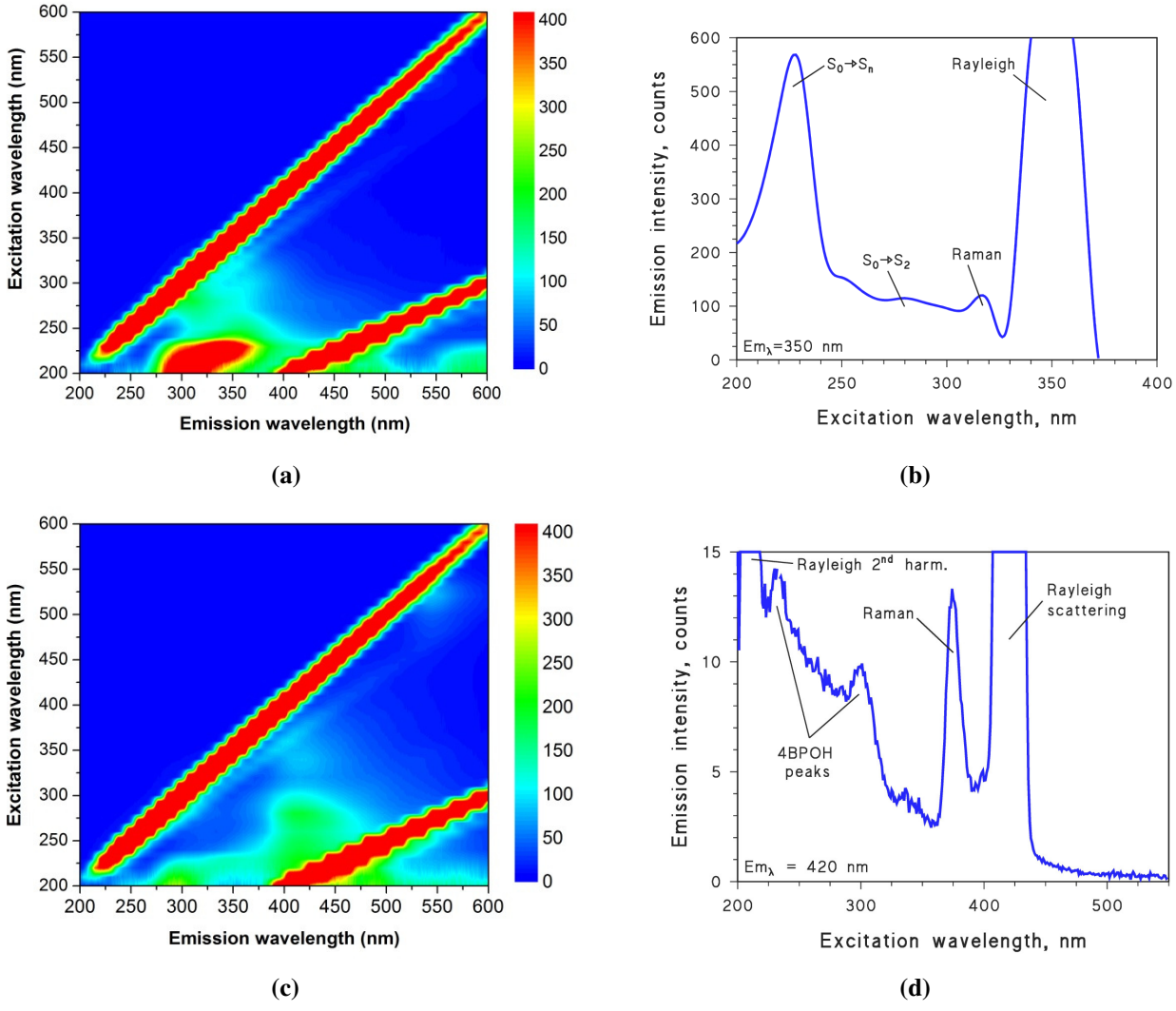

Figure 3. EEM spectra of 4HOBP in ACN (excitation slit width 10 nm, emission slit width 10 nm) at 4HOBP concentration values of 0.01 mM **(a)** and 0.1 mM **(c)**. **(b)** Excitation spectrum of 0.01 mM 4HOBP in ACN, corresponding to a fixed 350 nm emission wavelength ($S_2 \rightarrow S_0$ transition). S_n represents an energy state higher than S_2, or vibrationally excited S_2. **(d)** Excitation spectrum of 0.1 mM 4HOBP in ACN, corresponding to a fixed 420 nm emission wavelength ($S_1 \rightarrow S_0$). Note the two peaks at ~220 and ~290 nm, which are coherent with the absorption bands of 4HOBP (**Figure 1b**), and the presence of the second harmonic of the Rayleigh scattering.

The EEM spectrum of 4HOBP underwent important changes when increasing the substrate concentration. The intensity of the main fluorescence peak decreased, while a couple of new peaks appeared at Ex/Em = 200-220/400-500 nm and Ex/Em = 260-280/400-470 nm. Very interestingly, these peaks are in the same spectral region as "peak A" and "peak C" of humic substances.[10,11] By mere comparison with TD-DFT data, in both cases the emission interval could be compatible with a $T_1 \rightarrow S_0$ or a $S_1 \rightarrow S_0$ transition that are calculated at, respectively, 521 and 504 nm. Although it is unusual to detect a radiative $T_1 \rightarrow S_0$ transition (phosphorescence emission) at room temperature in solution, the emission wavelength interval compares well with the vibrationally resolved spectra of 4HOBP registered in ethanol glass at 77 K, which show peaks at 433, 450, 475, and 518 nm.[6] To better understand the nature of this radiative transition, 4HOBP emission spectra were measured in air, in pure oxygen and in oxygen-free atmosphere at different concentration values of 4HOBP in ACN. The rationale is that the T_1 state of 4HOBP undergoes energy transfer to O_2, which is in competition with the emission of radiation. The more important is the reaction with O_2, the faster is the deactivation of T_1 and the higher inhibition is expected for a $T_1 \rightarrow S_0$ radiative process. Indeed, the T_1 lifetime was about halved when passing from an O_2-free atmosphere to air, and it was decreased by an order of magnitude when passing from O_2-free to pure O_2.[3] As a consequence, under the hypothesis that the emission signal is due to a $T_1 \rightarrow S_0$ transition, one would expect the signal intensity to decrease by about one order of magnitude when passing from an O_2 - free to a pure O_2 atmosphere. The same effect would not necessarily be observed if the signal is due to a $S_1 \rightarrow S_0$ transition, because of the very short lifetime of the excited singlet states of 4HOBP.[3] The oxygen effect was studied on the 260-280/400-470 nm emission intensity ("C-like" peak), as the signal from the "A-like" peak was affected by the second harmonic of the Rayleigh scattering (see **Figure 3c**). The results are reported in **Figure 4**, which shows that the differences between O_2-free, aerated and pure-O_2 systems were within the experimental uncertainty. The unimportant effect of oxygen rules out the $T_1 \rightarrow S_0$ transition as the cause of the observed emission signal, that is rather assigned to a $S_1 \rightarrow S_0$ transition calculated at 504 nm, which alone is compatible with both the experimental emission wavelengths and the oxygen effect.

From the above discussion one gets that the intensity of the "humic-like" fluorescence peaks increased when increasing the concentration of 4HOBP, while the other two peaks showed a non-linear trend with 4HOBP concentration. On more quantitative grounds, **Figure 5** reports the fluorescence intensity at Ex/Em = 310/420 nm ("C-like" peak) and at Ex/Em = 230/330 nm (main fluorescence peak at low 4HOBP), as a function of 4HOBP concentration. The 310/420 nm signal increased almost linearly with 4HOBP concentration (black triangles in **Figure 5**), in agreement with the fact that the absorbance of the solution was relatively low at 310 nm and null at 420 nm (see **Figure 1b**). An important inner-filter effect on either excitation or emission is thus excluded.

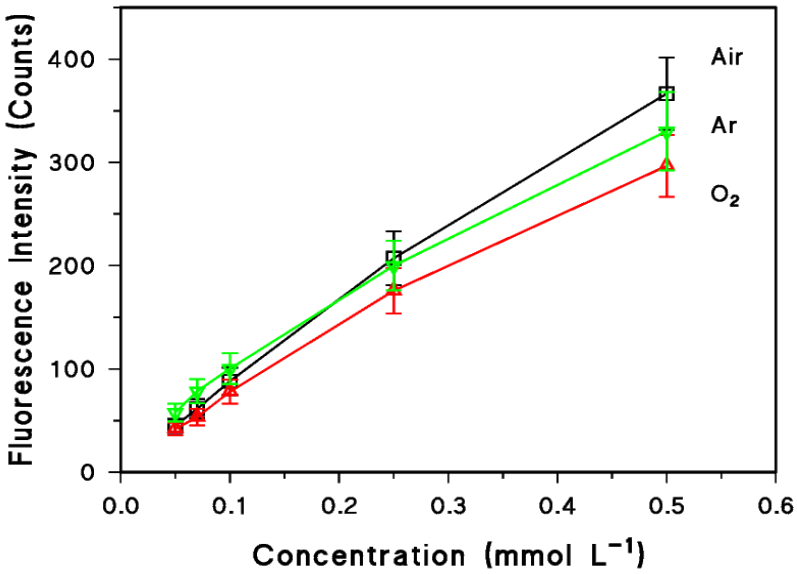

Figure 4. Fluorescence Intensity vs. Concentration of 4HOBP in ACN solutions, in air (black), O_2 atmosphere (red) and argon atmosphere (green). The fluorescence signal is that observed at Ex=300 nm / Em= 420 nm, using 10 nm slit widths in both excitation and emission. Error bars represent the standard errors of replicate experiments.

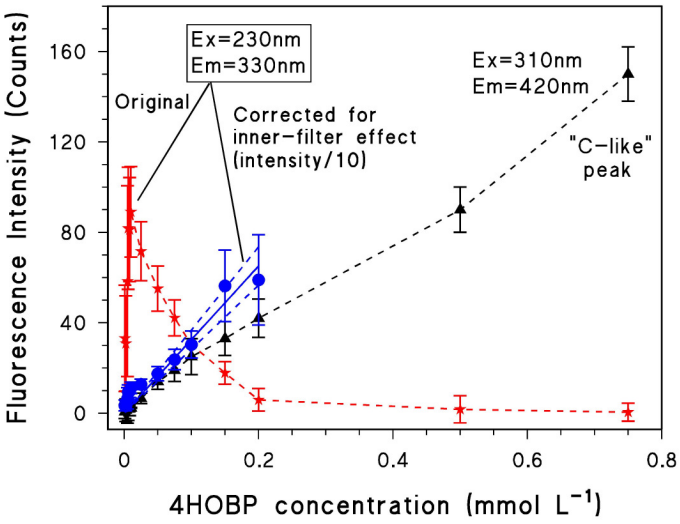

Figure 5. Fluorescence Intensity vs. Concentration of 4HOBP in ACN solutions, referred to different fluorescence peaks. The black triangles represent the so called "Humic-Like" C peak. As far as the other fluorescence peak is concerned, the red stars represent the raw emission data. The blue circles represent the emission intensity corrected for the inner-filter effect on excitation, and divided by 10 for scaling issues. Error bars represent the standard errors of replicate experiments. Slit width: 5 nm in excitation and 10 nm in emission.

The intensity of the 230/330 nm peak reached a maximum at 0.01 mM 4HOBP and decreased at higher 4HOBP concentration (red stars in **Figure 5**). The decrease might be accounted for by an inner-filter effect on excitation (λ_{ex}=230 nm, where there is important absorption by 4HOBP), while on the contrary 4HOBP is scarcely able to absorb radiation emitted at 330 nm (see **Figure 1b**). The issue is that the spectrofluorimeter detects the fluorescence emission from a region located in the center of the cuvette, which is reached by the incident (excitation) radiation after it has traveled for ~0.5 cm inside the solution. If we assume $p°(\lambda)$ as the incoming photon flux in solution, the photon flux of radiation that has traveled for a path length *b* can be expressed as follows:

$$p_b(\lambda) = p°(\lambda)\, 10^{-\varepsilon_{4HOBP}^{230nm}\, b\,[4HOBP]}$$

where $\varepsilon_{4HOBP}^{230nm}$ is the molar absorption coefficient of 4HOBP at 230 nm, [4HOBP] is the concentration of the substrate and *b* = 0.5 cm. By multiplying the fluorescence intensity data for the product $p°(\lambda)[p_b(\lambda)]^{-1}$ (>1) one can account for the inner-filter effect. The result of this procedure is represented as blue circles in **Figure 5**, showing that the trend with a maximum gets linearized when accounting for the solution absorbance. The correction did no longer work above 0.2 mM 4HOBP, probably because the raw emission intensity was too low and it was probably affected by a considerable uncertainty.

The EEM spectrum in 2-propanol (see Figure 2b in ref. 3) quite resembles that registered in ACN (see **Figure 3** in this work). The peaks found in 2-propanol were centered at excitation/emission wavelengths (Ex/Em) of: *(i)* 340/475 nm; *(ii)* 265/330 nm; *(iii)* 225/330 nm. The missing peak in 2-propanol is that interfered by the 2nd Rayleigh harmonic in ACN. The weak 340/475 nm peak could be compatible with a $S_1 \rightarrow S_0$ transition which is calculated at 505 nm (f=0.001), while the 265/330 and 225/330 peaks could be compatible with a $S_2 \rightarrow S_0$ transition that is calculated at 342 nm (f=0.600). Fluorescence in water is discussed in section 3.3.

3.2 Electronic structures of the excited states

The nature of the first two singlet excited states S_1 and S_2 and that of the first triplet state T_1 of 4HOBP was analyzed in terms of differential electronic density maps (**Figure 6**). The figure clearly shows that all three excited states correspond to charge-transfer from the hydroxyphenyl moiety, involving both the phenyl π and the hydroxyl lone pair electrons, towards the anti-bonding orbitals located on the phenyl (π*) and carbonyl groups (π_{CO}*). Some contribution of an excitation from the non-bonding/lone pair n_{CO} is also present. On the basis of these data we can asses that these excited states correspond to mixed n-π* and π-π* configurations. Differences can only be found by inspection of the coefficients and nature of the configurations that are reported as ESI.

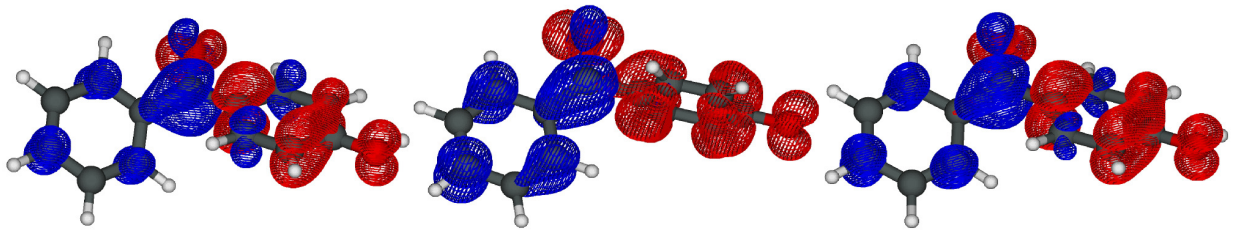

Figure 6. Differential electronic density maps for the states T_1 (left), S_1 (center) and S_2 (right), with respect to S_0. Red areas correspond to a reduction in the electronic density, blue areas correspond to an increase in the electronic density.

The electronic properties of the excited states are also well illustrated by the change in the electrostatic potential V compared to that of the ground state (**Figure 7**). **Figure 7a** (electrostatic potential in ACN) clearly shows that in all the excited states, and particularly in S_1, the hydroxyphenyl moiety assumes an acid (and electrophilic) character while the benzoyl moiety (and particularly the carbonyl group) becomes more basic (more nucleophilic), as a result of the partial charge-transfer nature of these excited states. It is noticeable that the oxygen atom of the hydroxyl group, which shows a small basic character in S_0 (the small blue area opposite to the hydrogen and corresponding to the lone pair areas), becomes essentially neutral in S_1 (the blue area becomes white) or less basic in T_1 (the blue area becomes smaller). The changes in the chemical and electrostatic properties of the excited states are even more evident in water (**Figure 7b**). All the excited states show more acidic hydroxyphenyl moieties, with a loss of the basic character of the hydroxyl oxygen atoms. Excited states in 2-propanol show similar behavior (see **Figure ESI6**). These electronic properties are expected to have consequences on the acid properties of the excited states.

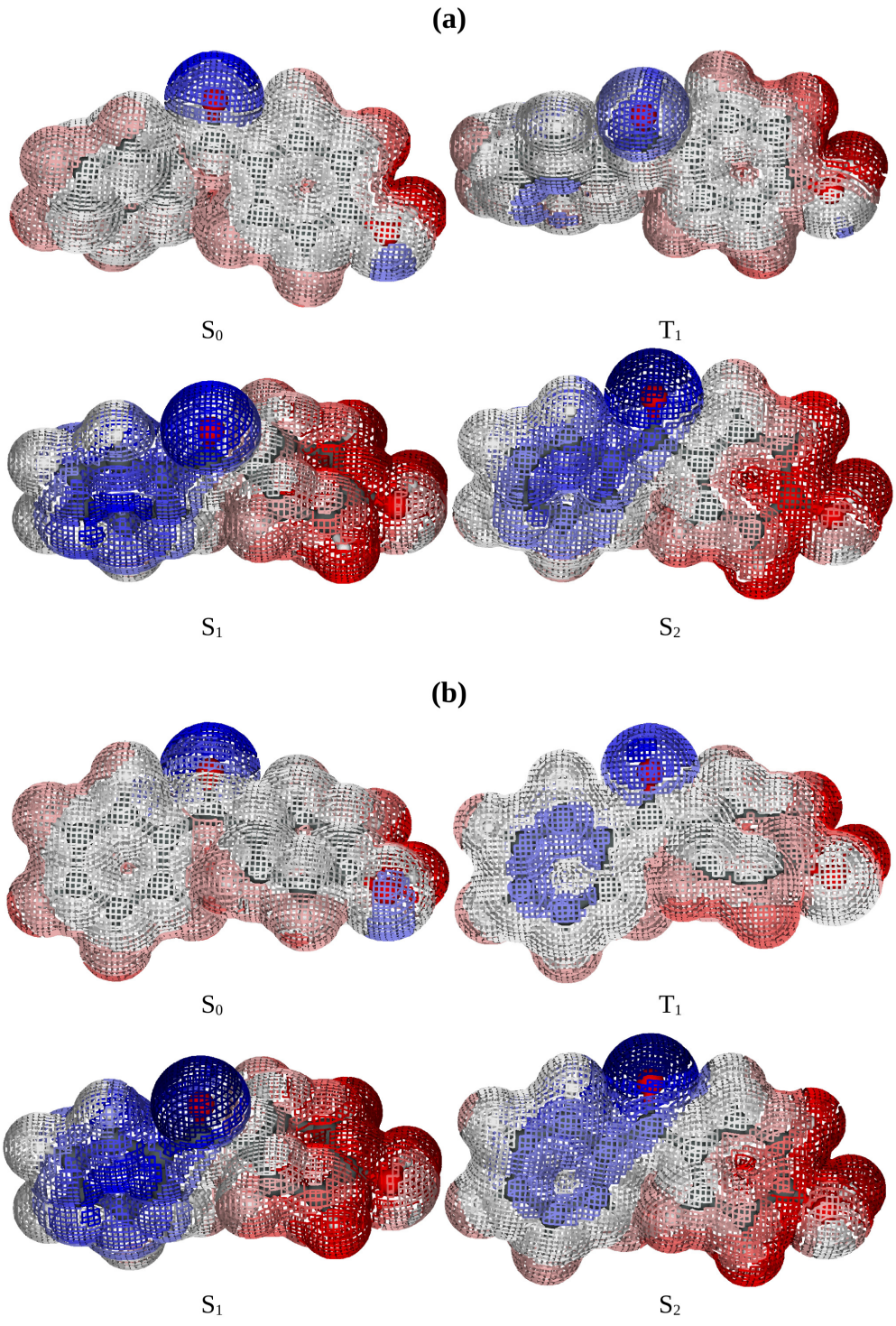

Figure 7. Electrostatic potential V on the Van der Waals surfaces of the S_0, T_1, S_1, and S_2 states in ACN **(a)** and water **(b)**. Red areas correspond to positive V values (acid/electrophilic character), blue areas correspond to negative V values (basic/nucleophilic character).

3.3 Acid properties

The exact calculation of the pK_a of an acid is quite a though challenge.[53] In this work we have found a reasonable model that allowed us to calculate the pK_a of the ground state of 4HOBP in water, in good agreement with the experimental findings. Our pK_a value, 8.3, well compares with 7.9 reported by Bhasikutta *et al.*[54] or with 8.5 reported by Porter and Suppan.[8] Moreover, a value of 8.21 can be estimated with the Hammett equation.[55] Our model consists in the use of the water complexes of the undissociated 4HOBP and of the anionic $4OBP^-$, and of a water molecule and an ossonium cation:

$$[4HOBP\ (H_2O)_3]\ +\ (H_2O)_4\ \leftrightarrows\ [4OBP\ (H_2O)_3]^-\ +\ [H_3O\ (H_2O)_3]^+ \quad (1)$$

Figures of all complexes are reported as ESI (**ESI7**, **ESI8**). The same protocol was used to calculate the deprotonation equilibria for the S_1 and T_1 states. Using 2-propanol molecules, we calculated also the deprotonation equilibria of S_0, S_1 and T_1 in this alcoholic solvent. The results are collected in **Table 1**.

Table 1. Equilibrium constants and pK_a (in parenthesis) for the proton transfer from 4HOBP to the solvents water and 2-propanol.

	Water	**2-Propanol**
$\mathbf{S_0}$	$9.0\ 10^{-11}$ (8.3)	$9.6\ 10^{-13}$ (12.0)
$\mathbf{S_1}$	$1.5\ 10^{-1}$ (-0.9)	$2.4\ 10^{-1}$ (0.6)
$\mathbf{T_1}$	$4.9\ 10^{-2}$ (-0.4)	$1.5\ 10^{-2}$ (1.8)

Coherently with what was anticipated in paragraph 3.2, both the excited states S_1 and T_1 show a strong increase of the acidity compared to the ground state: the first singlet state in water is one billion times more acidic than the ground state, and the effect is even larger in 2-propanol where S_1 is one hundred billion times more acidic than S_0. The triplet states show almost the same strong increase of the acidity. The calculation results are in reasonable agreement with experimental findings in water, according to which both 4HOBP-S_1 and 4HOBP-T_1 have $pK_a < 0$.[8] By contrast, despite the strong effect of the electronic excitation, the excited states of 4HOBP in 2-propanol still behave as weak acids. The deprotonation of the 4HOBP-S_1 and 4HOBP-T_1 states in 2-propanol does not seem to be competitive with respect to the other decay processes, as testified by the similarity between the EEM spectra [3] registered in 2-propanol and in ACN where the deprotonation is not possible, being the latter solvent not basic.

The acidity of 4HOBP-S_1 compared to the ground state has important implications for the fluorescence of 4HOBP in water. Indeed, in a wide range of pH conditions the ground state would be undissociated but the S_1 state, produced after radiation absorption, would quickly undergo deprotonation. The absorption spectra of 4HOBP at pH 1 (occurrence of the undissociated form), in ~neutral pH conditions (mixture of 4HOBP and $4OBP^-$ with a prevalence of the former) and at pH 10 ($4OBP^-$) are reported in **Figure 8a**. The occurrence of the anion $4OBP^-$ at pH 10 and its absorption spectrum agree well with the computations: the calculated absorption spectrum of $4OBP^-$ (**Figure 8b**, blue line) shows two peaks at 346 and 257 nm that correspond to the experimental maxima found at 348 and 250 nm.

Figure 9 reports the fluorescence spectra obtained upon excitation of 4HOBP solutions at pH 1.0, 6.1 and 10.0. The spectra were measured at excitation wavelengths of 230 (**9a**), 258 (**9b**) and 311 nm (**9c**), at which wavelengths the acidic form of 4HOBP has the same molar absorption coefficients as the basic one (see spectra at pH 1 and 10 in **Figure 8a**). Some of the peaks in the spectra correspond to Rayleigh or Raman signals. In the case of excitation at 230 nm one should consider the 4HOBP emission band at ~ 320 nm, which has intensity order pH 1 ~ pH 10 > natural pH (**Figure 9a**). The same trend is observed with the emission band around 360 nm produced upon excitation at 258 nm (**Figure 9b**). In the case of the emission above 400 nm upon excitation at 311 nm, one has the intensity order pH 10 > pH 1 > natural pH (**Figure 9c**). In all the cases the solution at pH 10 showed significant emission which implies that, at equal absorbance, the basic form $4OBP^-$ is able to emit fluorescence radiation from its excited singlet states at a similar or even higher extent than the acidic form 4HOBP. In contrast, the solution at the natural pH always showed the lowest fluorescence intensity. At ~neutral pH, radiation absorption by ground-state 4HOBP (pK_a ~ 8) yields the molecule in an excited state (generically indicated as 4HOBP*, $pK_a < 0$), which undergoes deprotonation in competition with fluorescence emission. Considering that the efficiency of fluorescence emission from $4OBP^-$* is similar to or even higher than that from 4HOBP*, it is unlikely that the deprotonation of 4HOBP* yields $4OBP^-$*. The low fluorescence emission of 4HOBP at the natural pH is more plausibly accounted for by deprotonation of 4HOBP* to give ground-state $4OBP^-$, without photon emission. In acidic solution the deprotonation of 4HOBP* is inhibited to some extent, which leads to an increase in the fluorescence intensity. In basic solution, the ground-state $4OBP^-$ is radiationally excited to $4OBP^-$*, which does not undergo acid-base equilibria and emits fluorescence photons with good efficiency.

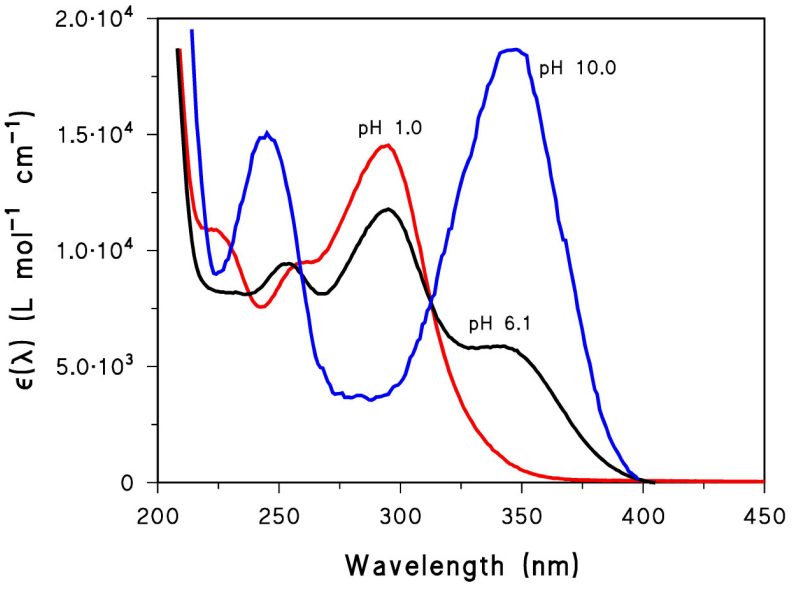

(a)

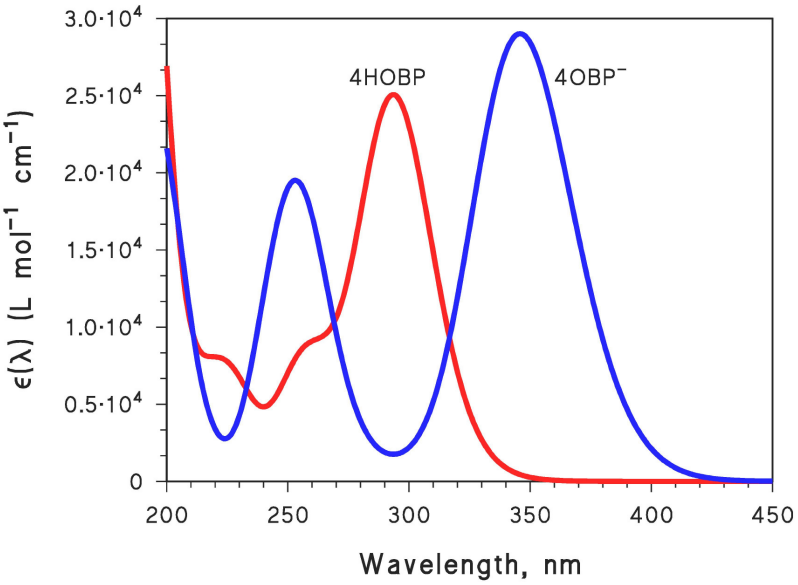

(b)

Figure 8. (a) Absorption spectra of 0.1 mM 4HOBP in water solution, at different pH values: pH 1.0 red line (adjusted with $HClO_4$), pH 10.0 blue line (adjusted with NaOH) and natural pH (not adjusted, pH 6.1) black line. **(b)** Calculated absorption spectra in water of the anion $4OBP^-$ (blue line) and of undissociated 4HOBP (red line).

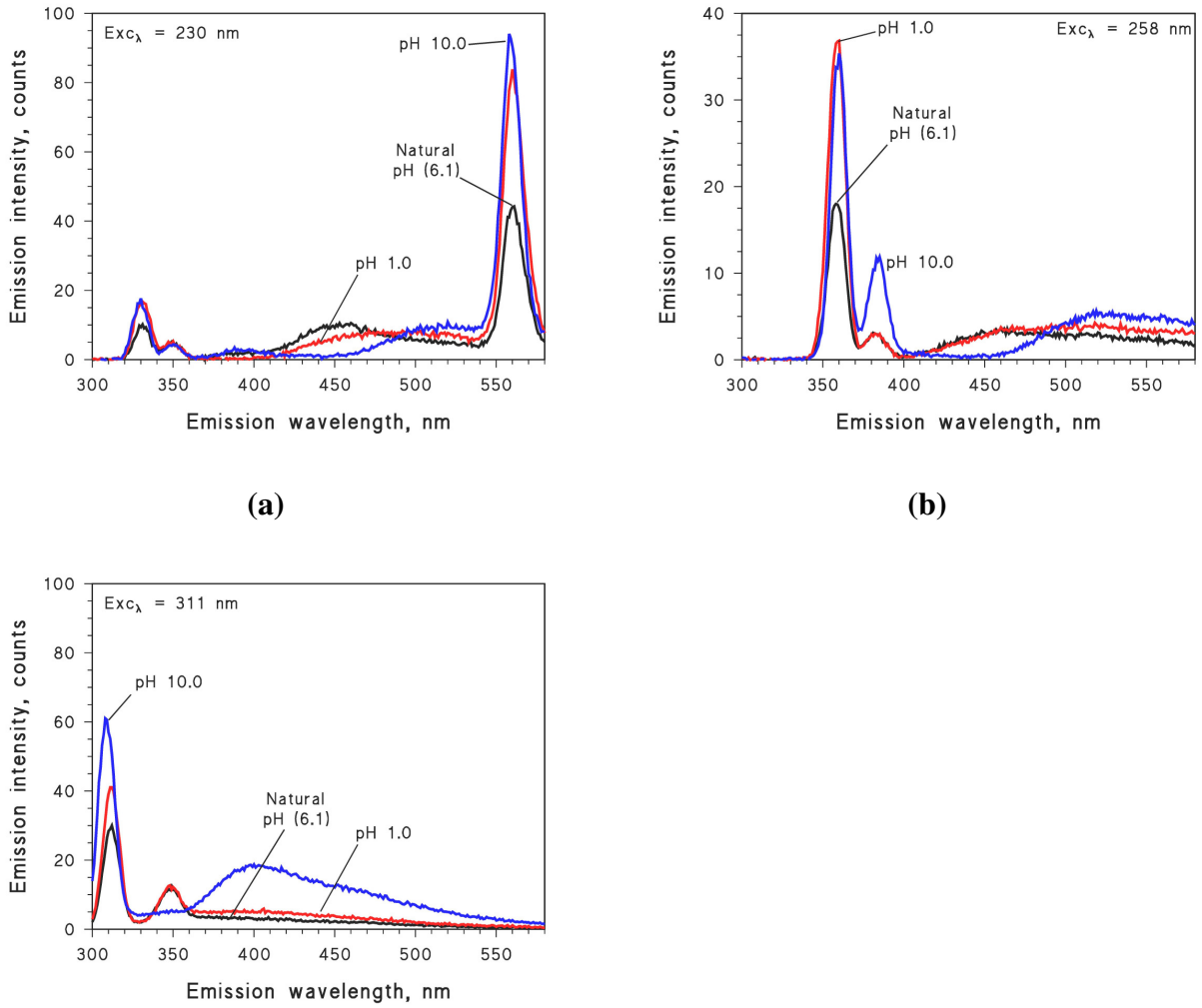

Figure 9. Fluorescence emission spectra of 4HOBP 0.05 mM in aqueous solution, excited at 230 **(a)**, 258 **(b)** and 311 nm **(c)**, at different pH values: pH 1.0 red line (adjusted with $HClO_4$), pH 10.0 blue line (adjusted with NaOH) and natural pH (6.1, not adjusted) black line.

4. Conclusions

The fluorescence spectrum of 4-hydroxybenzophenone (4HOBP) shows signals at two different emission wavelengths, which is not typical and is accounted for by the fact that 4HOBP does not follow Kasha's rule. Actually, both the S_1 and S_2 excited singlet states account for the observed fluorescence emission, with S_2 giving the most intense signals. The EEM spectrum shows two couples of fluorescence peaks; the first couple is centered at emission wavelengths ~300-350 nm, corresponding to a $S_2 \rightarrow S_0$ transition. The most intense peak has Ex/Em ~200-230/280-370 nm,

with the excitation wavelength corresponding to a transition from S_0 to S_5 or S_6, or to a highly excited vibrational state of S_2. The excitation spectrum supports the former hypothesis. This peak is quite intense at low concentration but undergoes a significant inner-filter effect that produces a decrease in intensity above 0.01 mM 4HOBP. The less intense peak of this couple has Ex/Em ~270-300/320-360 nm, and it corresponds to a $S_0 \rightarrow S_2$ transition in excitation. The other couple of peaks has Ex/Em ~ 200-220/400-500 nm and Ex/Em ~ 260-280/400-470 nm, and in both cases the emission interval is consistent with a $S_1 \rightarrow S_0$ transition. These peaks are interesting because they fall in the respective regions of the "peak A" and "peak C" of humic substances, and because aromatic carbonyls in general, and benzophenones in particular, are well-known components of humic matter. Because the most intense peak arising from the $S_2 \rightarrow S_0$ transition suffers from an inner-filter effect, and the "A-like" and "C-like" peaks are not very intense, there are concentration intervals where 4HOBP shows quite low radiation emission. This could be one of the reasons why the fluorescence of 4HOBP has been described only recently. The fluorescence of 4HOBP can be observed in aprotic or poorly protic solvents, and also in aqueous solution. However, in water the fluorescence of 4HOBP is more intense at acidic or basic pH compared to ~neutral solutions. The likely reason is that 4HOBP-S_0 is a relatively weak acid (pK_a ~8), while its excited states (4HOBP*) are strong acids. In ~neutral solution, ground-state 4HOBP is radiationally excited to 4HOBP* that undergoes deprotonation to $4OBP^-$, in competition with fluorescence emission. In acidic solution the fluorescence is more intense because the deprotonation of 4HOBP* is less efficient. In basic solution, ground-state $4OBP^-$ is excited to $4OBP^-$* that, not being involved in proton exchange, yields back $4OBP^-$ through photon emission.

Acknowledgements

GG acknowledges financial support by Università di Torino - Local funding. DV acknowledges financial support by MIUR - PNRA.

Supplementary data

Supplementary data associated with this article can be found, in the online version, at http://

References

1. M. I. Sancho, A. H. Jubert, S. E. Blanco, F. H. Ferretti and E. A. Castro, Determination of dissociation constants of *p*-hydroxybenzophenone in aqueous organic mixtures – Solvent effects, *Can. J. Chem.*, 2008, **86**, 462-469.
2. Y. Du, J. D. Xue, C. S. Ma, W. M. Kwok and D. L. Phillips, Time-resolved resonance Raman and density functional theory study of the deprotonation reaction of the triplet state of *para*-hydroxybenzophenone in mixed acetonitrile/water solutions, *J. Raman Spectrosc.*, 2008, **39**, 1518-1525.
3. F. Barsotti, M. Brigante, M. Sarakha, V. Maurino, C. Minero and D. Vione, Photochemical processes induced by the irradiation of 4-hydroxybenzophenone in different solvents, *Photochem. Photobiol. Sci.*, 2015, **14**, 2087-2096.
4. M. Hoshino and M. Koizumi, Order of quencher participation in photochemistry. I. Proton transfer from the excited p-hydroxybenzophenone in mixed solvents of cyclohexane and alcohols, *Bull. Chem. Soc. Japan*, 1972, **45**, 2731-2736.
5. D. K. Palit, Photophysics and excited state relaxation dynamics of p-hydroxy and p-amino-substituted benzophenones: a review, *Res. Chem. Intermed.*, 2005, **31**, 205-225.
6. A. C. Bhasikuttan, A. K. Singh, D. K.Palit, A. V. Sapre and J.P. Mittal, Laser flash-photolysis studies on the monohydroxy derivatives of benzophenone, *J. Phys. Chem. A*, 1998, **102**, 3470-3480.
7. A. Beckett and G. Porter, Primary photochemical processes in aromatic molecules. Part 10. Photochemistry of substituted benzophenones, *Trans. Faraday Soc.*, 1963, **59**, 2051-2057.
8. G. Porter and P. Suppan, Primary photochemical processes in aromatic molecules. Part 12. Excited states of benzophenone derivatives, *Trans. Faraday Soc.*, 1965, **61**, 1664-1673.
9. P. K. Das, M. V. Encinas and J. C. Scaiano, Laser flash photolysis study of the reactions of carbonyl triplets with phenols and photochemistry of p-hydroxypropiophenone, *J. Am. Chem. Soc.*, 1981, **103**, 4154-4162.
10. P. G. Coble, Characterization of marine and terrestrial DOM in seawater using excitation-emission spectroscopy, *Mar. Chem.*, 1996, **51**, 325-346.
11. X. Luciani, S. Mounier, H. H. M. Paraquetti, R. Redon, Y. Lucas, A. Bois, L. D. Lacerda, A. Raynaud and A. Ripert, Tracing of dissolved organic matter from the SEPETIBA Bay (Brazil) by PARAFAC analysis of total luminescence matrices, *Mar. Environ. Res.*, 2008, **65**, 148-157.
12. K. R. Murphy, C. A. Stedmon, T. D. Waite and G. M. Ruiz, Distinguishing between terrestrial and autochthonous organic matter sources in marine environments using fluorescence spectroscopy, *Mar. Chem.*, 2008, **108**, 40-58.
13. R. K. Henderson, A. Baker, K. R. Murphy, A. Hamblya, R. M. Stuetz and S. J. Khan, Fluorescence as a potential monitoring tool for recycled water systems: A review, *Water Res.*, 2009, **43**, 863-881.

14. L. Jorgensen, C. A. Stedmon, T. Kragh, S. Markager, M. Middelboe and M. Sondergaard, Global trends in the fluorescence characteristics and distribution of marine dissolved organic matter, *Mar. Chem.*, 2011, **126**, 139-148.
15. E. De Laurentiis, M. Minella, V. Maurino, C. Minero, M. Brigante, G. Mailhot and D. Vione, Photochemical production of organic matter triplet states in water samples from mountain lakes, located below or above the tree line, *Chemosphere*, 2012, **88**, 1208-1213.
16. F. Barsotti, G. Ghigo and D. Vione, Computational assessment of the fluorescence emission of phenol oligomers: A possible insight into the fluorescence properties of humic-like substances (HULIS), *J. Photochem. Photobiol. A: Chem.*, 2016, **315**, 87-93.
17. D. Smejkalova and A. Piccolo, Aggregation and disaggregation of humic supramolecular assemblies by NMR diffusion ordered Spectroscopy (DOSY-NMR), *Environ. Sci. Technol.*, 2008, **42**, 699-706.
18. J. Peuravuori, NMR spectroscopy study of freshwater humic material in light of supramolecular assembly, *Environ. Sci. Technol.*, 2005, **39**, 5541-5549.
19. D. E. Latch and K. McNeill, Microheterogeneity of singlet oxygen distributions in irradiated humic acid solutions, *Science*, 2006, **311**, 1743-1747.
20. M. Grandbois, D. E. Latch and K. McNeill, Microheterogeneous concentrations of singlet oxygen in natural organic matter isolate solutions, *Environ. Sci. Technol.*, 2008, **42**, 9184-9190.
21. M. Minella, M. P. Merlo, V. Maurino, C. Minero and D. Vione, Transformation of 2,4,6-trimethylphenol and furfuryl alcohol, photosensitised by Aldrich humic acids subject to different filtration procedures. *Chemosphere*, 2013, **90**, 306-311.
22. E. Appiani and K. McNeill, Photochemical production of singlet oxygen from particulate organic matter, *Environ. Sci. Technol.*, 2015, **49**, 3514-3522.
23. S. Canonica, U. Jans, K. Stemmler and J. Hoigné, Transformation kinetics of phenols in water - Photosensitization by dissolved natural organic material and aromatic ketones, *Environ. Sci. Technol.*, 1995, **29**, 1822-1831.
24. C. M. Sharpless and N. V. Blough, The importance of charge-transfer interactions in determining chromophoric dissolved organic matter (CDOM) optical and photochemical properties, *Environ. Sci.: Processes Impacts*, 2014, **16**, 654-671.
25. P. J. Wagner, R. J. Truman, A. E. Puchalski, R. Wake, Extent of charge transfer in the photoreduction of phenyl ketones by alkylbenzenes, *J. Am. Chem. Soc.* 1986, **108**, 7727-7738
26. F. Jensen, Introduction to Computational Chemistry, John Wiley & Sons, NY, 1999, ISBN 0-471-98425-98426.
27. R.G. Parr, W. Yang, Density Functional Theory of Atoms and Molecules, Oxford University Press, 1989.
28. W. Kohn, A.D. Becke, R.G. Parr, Density functional theory of electronic structure, *J. Phys. Chem.* 1996, **100**, 12974-12980.

29. W. J. Hehre, R. Ditchfield, J. A. Pople, Self-consistent molecular orbital methods. XII. Further extensions of Gaussian-type basis sets for use in molecular orbital studies of organic molecules, *J. Chem. Phys.* 1972, **56**, 2257-2261.
30. T. Clark, J. Chandrasekhar, G.W. Spitznagel, P.v.R. Schleyer, Efficient diffuse function-augmented basis-sets for anion calculations. 3. The 3-21+G basis set for 1st-row elements, Li-F, *J. Comput. Chem.* 1983, **4**, 294-301.
31. B. Mennucci, J. Tomasi, Continuum solvation models: a new approach to the problem of solute's charge distribution and cavity boundaries, *J. Chem. Phys.* 1997, **106**, 5151-5158.
32. M. Cossi, N. Rega, G. Scalmani, V. Barone, Polarizable dielectric model of solvation with inclusion of charge penetration effects, *J. Chem. Phys.* 2001, **114**, 5691-5570.
33. A. V. Marenich, C. J. Cramer, D. G. Truhlar, Universal solvation model based on solute electron density and on a continuum model of the solvent defined by the bulk dielectric constant and atomic surface tensions, *J. Phys. Chem. B* 2009, **113**, 6378–6396.
34. A. V. Marenich, C. J. Cramer, D. G. Truhlar, Performance of SM6, SM8, and SMD on the SAMPL1 test set for the prediction of small-molecule solvation free energies, *J. Phys. Chem. B* 2009, **113**, 4538-4543.
35. R. Bauernschmitt, R. Ahlrichs, Treatment of electronic excitations within the adiabatic approximation of time dependent density functional theory, *Chem. Phys. Lett.* 1996, **256**, 454-464.
36. A. Dreuw, M. Head-Gordon, Single-reference ab initio methods for the calculation of excited states of large molecules, *Chem. Rev.* 2005, **105**, 4009-4037.
37. D. Jacquemin, E. A. Perpète, O. A. Vydrov, G. E. Scuseria, C. Adamo, Assessment of long-range corrected functionals performance for n→π* transitions in organic dyes, *J. Chem. Phys.* 2007, **127**, 094102.
38. D. Jacquemin, V. Wathelet, E. A. Perpète, C. Adamo, Extensive TD-DFT benchmark: Singlet-excited states of organic molecules, *J. Chem. Theory Comput.* 2009, **5**, 2420-2435.
39. A. D. Laurent and D. Jacquemin, TD-DFT Benchmarks: A Review, *Int. J. Quantum Chem.* 2013, **113**, 2019–2039.
40. A. Charaf-Eddin, A. Planchat, B. Mennucci, C. Adamo, and D. Jacquemin, Choosing a functional for computing absorption and fluorescence band shapes with TD-DFT, *J. Chem. Theory Comput.* 2013, **9**, 2749-2760. ,
41. J. P. Perdew, K. Burke, M. Ernzerhof, Generalized gradient approximation made simple, *Phys. Rev. Lett.*, 1996, **77**, 3865-3868.
42. J. P. Perdew, K. Burke, M. Ernzerhof, Errata: Generalized gradient approximation made simple, *Phys. Rev. Lett.*, 1997, **78**, 1396.
43. C. Adamo, V. Barone, Toward reliable density functional methods without adjustable parameters: The PBE0 model, *J. Chem. Phys.*, 1999, **110**, 6158-6169.

44. Gaussian Web site, page: http://www.gaussian.com/g_whitepap/tn_uvvisplot.htm, consulted 13 June 2016.
45. P. J. Stephens, N. Harada, ECD Cotton effect approximated by gaussian curve and other methods, *Chirality* 2010, **22**, 229-233.
46. A. D. McLean, G. S. Chandler, Contracted Gaussian basis sets for molecular calculations. I. Second row atoms, Z=11–18, *J. Chem. Phys.* 1980, **72**, 5639-5348.
47. M. J. Frisch, G. W. Trucks, H. B. Schlegel, G. E. Scuseria, M. A. Robb, J. R. Cheeseman, G. Scalmani, V. Barone, B. Mennucci, G. A. Petersson, H. Nakatsuji, M. Caricato, X. Li, H. P. Hratchian, A. F. Izmaylov, J. Bloino, G. Zheng, J. L. Sonnenberg, M. Hada, M. Ehara, K. Toyota, R. Fukuda, J. Hasegawa, M. Ishida, T. Nakajima, Y. Honda, O. Kitao, H. Nakai, T. Vreven, J. A. Montgomery Jr., J. E. Peralta, F. Ogliaro, M. Bearpark, J. J. Heyd, E. Brothers, K. N. Kudin, V. N. Staroverov, R. Kobayashi, J. Normand, K. Raghavachari, A. Rendell, J. C. Burant, S. S. Iyengar, J. Tomasi, M. Cossi, N. Rega, J. M. Millam, M. Klene, J. E. Knox, J. B. Cross, V. Bakken, C. Adamo, J. Jaramillo, R. Gomperts, R. E. Stratmann, O. Yazyev, A. J. Austin, R. Cammi, C. Pomelli, J. W. Ochterski, R. L. Martin, K. Morokuma, V. G. Zakrzewski, G. A. Voth, P. Salvador, J. J. Dannenberg, S. Dapprich, A. D. Daniels, Ö. Farkas, J. B. Foresman, J. V. Ortiz, J. Cioslowski, D. J. Fox, Gaussian 09, Gaussian, Inc., Wallingford, CT, 2009.
48. G. Schaftenaar, J. H. Noordik, Molden: a pre- and post-processing program for molecular and electronic structures, *J. Comput.-Aided Mol. Des.* 2000, **14**, 123-134.
49. M. Kasha, Characterization of electronic transitions in complex molecules, *Discuss Faraday Soc.* 1950, **9**, 14-19.
50. M. Chergui, Empirical rules of molecular photophysics in the light of ultrafast spectroscopy, *Pure Appl. Chem.* 2015, **87**, 525-536.
51. T. Itoh, Fluorescence and phosphorescence from higher excited states of organic molecules, *Chem Rev.* 2012, **112**, 4541-4568.
52. S. Nagaoka, M. Fujita, T. Takemura, H. Baba, Fluorescence from an upper excited state of *o*-hydroxybenzaldehyde in the vapor phase, *Chem. Phys. Lett.* 1986, **123**, 489-492.
53. T. Matsui, T. Baba, K. Kamiyad, Y. Shigetab, An accurate density functional theory based estimation of pKa values of polar residues combined with experimental data: from amino acids to minimal proteins, *Phys. Chem. Chem. Phys.*, 2012, **14**, 4181–4187.
54. A. C. Bhasikutta, A. K. Singh, D. K. Palit, A. V. Sapre, J. P. Mittal, Study of spectral characteristics, kinetics, and equilibria of radicals derived from hydroxy benzophenones, *J. Phys. Chem. A* 1999, **103**, 4703-4711.
55. C. Hansch, A. Leo, R. W. Taft, A survey of Hammett substituent constants and resonance and field parameters, *Chem. Rev.*, 1991, **91**, 165-195.